Impact of doping on bonding energy hierarchy and melting of phase change materials

Jie Liu,[1,2,3,a),b)] Evan Wang,[3,4,a)] Yunqi Zhao,[3,b)] Xu Xu,[3] Jeong-Sun Moon,[5] and M. P. Anantram[3,b)]
[1]*College of Electrical and Information Engineering, Hunan University, Changsha, China*
[2]*National Supercomputing Center in Changsha, Hunan Province, China*
[3]*Department of Electrical Engineering, University of Washington, Washington, Seattle 98195, USA*
[4]*Department of Electrical Engineering, Stanford University, Stanford, California 94305, USA*
[5]*HRL Laboratories, Malibu, California 90265, USA*

(Received 11 May 2018; accepted 21 August 2018; published online 5 September 2018)

The impact of doping on the bonding energy hierarchy and melting point of phase change material germanium telluride is studied. The underlying bonding energy decomposition is based on density functional theory calculations. It is shown that doping can influence the bonding energy hierarchy to lower the melting temperature and latent heat of fusion. Conversely, doping slightly increases the specific heat capacity. Nevertheless, doping induces a net reduction in energy consumption for the "reset" operation of phase change memory devices. This bonding energy analysis is three to four orders of magnitude more computationally efficient than the widely used *ab initio* molecular dynamics simulations. It is expected that this approach could be useful for next-generation high-throughput simulation-based phase change material design and optimization. *Published by AIP Publishing.*
https://doi.org/10.1063/1.5039831

I. INTRODUCTION

Phase change memory is a promising non-volatile data storage technology due to its ultra-fast operation speed,[1,2] sub-10 nm scalability,[3–5] multi-level data storage capability,[6] long data retention time, and high read and write operation cycle endurance.[7,8] Overall, phase change memory technologies exhibit favorable scaling with respect to major performance metrics.[9–11] Therefore, it has attracted significant attention in the past few decades for both electrical and optical device applications.[7,8,12,13] In electrical/optical phase change memory devices, the "reset" operation is achieved by first applying a current/laser pulse with short duration and high amplitude to melt the crystalline (*c*-) phase change material (PCM), then immediately quenching into the amorphous (*a*-) phase. The corresponding "set" operation is achieved by applying a long duration and moderate amplitude current/laser pulse to recrystallize the *a*-PCM back into *c*-PCM. The electrical/optical property contrast between these two phases is utilized to store data in a non-volatile manner.

Historically, the two most serious obstacles to large-scale application of phase change memory technologies were high "reset" energy and slow "set" speed.[7,8] Fortunately, recent research has shown that by reducing the stochasticity of PCM crystal nucleation, the "set" operation time can be reduced below 1 ns.[1] Such short switching times enable ultra-fast, GHz-level device speeds comparable to dynamic random-access memory (DRAM) and static random-access memory (SRAM).

In contrast, the issue of high "reset" energy consumption has yet to be resolved. In order to switch *c*-PCM into *a*-PCM, the active PCM region must be heated from room temperature up to the PCM's melting temperature (e.g., 725 °C for GeTe, and 632 °C for $Ge_2Sb_2Te_5$).[14] During this energy-consuming step (heating and melting), over 90% of the "reset" operation energy is wasted as thermal flux into the electrodes and substrate.[9]

A significant amount of experimental and theoretical research has been conducted to reduce the "reset" energy. This work can be classified into two categories—indirect and direct methods. Indirect methods sidestep the problem of high melting temperature and instead focus on reducing the wasted thermal flux, with approaches such as thermal boundary resistance (TBR)[15,16] and carbon nanotube (CNT) electrodes.[17] Preliminary results show potential "reset" energies on the order of femto-Joules, an improvement of 2–3 orders of magnitude compared to state-of-the-art, commercial PCM devices.[9,17] However, such indirect methods encounter key challenges: techniques to reliably fabricate CNT electrodes in large-scale PCM devices are still immature,[17] and the reduction of thermal flux into the electrodes is restricted to the fundamental limit posed by the Wiedemann-Franz law.[7]

In contrast, direct methods reduce the "reset" energy by suppressing the melting temperature through techniques such as super-lattice structure,[18] interfacial energy,[14,19] pressure,[20,21] and doping.[22,23] Among these methods, doping is one of the most convenient choices due to its compatibility with established semiconductor processes. Doping with a wide variety of atomic species (e.g., Si, C, O, N, Bi, Ag, Cd, In, Sn) has been demonstrated on chalcogenide PCMs such as GeTe, $Ge_2Sb_2Te_5$, and Sb_2Te_3.[22–32] However, existing research on doping PCM primarily relies on the "trial-and-error" method. Given the vast number of dopant species and PCM stoichiometries, it is a daunting task to search the entire set of possible combinations. Despite the physical insights offered, screening material combinations with methods such

[a)]J. Liu and E. Wang contributed equally to this work.
[b)]Authors to whom correspondence should be addressed: jie_liu@hnu.edu.cn, liujie@uw.edu; zhaoyq@uw.edu; and anant@uw.edu

as *ab initio* molecular dynamics (AIMD) are computationally intractable.[33–35] High-throughput simulation-based optimization of next-generation PCM devices[36,37] requires efficient methods that quantitatively link the macroscopic melting temperature with microscopic governing physics.

As an early-stage attempt to develop such techniques, this paper investigates the relationship between the doping-induced change in macroscopic melting temperature and the doping-induced change in the microscopic bonding energy hierarchy. Here, we focus on the prototypical binary PCM, germanium telluride (GeTe). In Sec. II, the methodology is introduced. In Sec. III, the results are shown. In Sec. IV, the computational costs are discussed. Sections V and VI present the discussion and conclusion, respectively.

II. ANALYSIS METHODOLOGY

The multi-scale methodology consists of three parts. First, density functional theory (DFT) is used to analyze the microscopic electronic structure properties (Secs. II A–II C). Next, DFT-based AIMD is used to analyze the doping-induced change in the melting temperature, ΔT_m (Sec. II D). Finally, a time-dependent finite element method (TD-FEM) is used to translate reduced PCM melting temperatures into improvements in phase change memory device performance (Sec. II E).

A. Density functional theory

We perform *ab initio* DFT calculations using the SIESTA package.[38] The plane wave cutoff is chosen to be 100.0 Ry. The generalized gradient approximation (GGA) of Perdew, Burke, and Ernzerhof (PBE) is used to approximately model the exchange-correlation effects.[39] The double-zeta plus polarization pseudo-atomic orbitals (PAOs) are used for all atoms. At the boundaries of the supercell, periodic boundary conditions (PBCs) are applied. The self-consistent field (SCF) electronic structure convergence criterion of the DFT calculation is set to 0.1 meV. The convergence criterion of the conjugate gradient (CG) lattice structure relaxation is set to 40 meV/Å.

B. Bonding energy analysis

The total energy computed using DFT is

$$E = \sum_{\mu\nu} H_{\mu\nu}\rho_{\mu\nu} - \frac{1}{2}\int V^H(\mathbf{r})\rho(\mathbf{r})d^3\mathbf{r} + \int (\epsilon^{xc}(\mathbf{r}) - V^{xc}(\mathbf{r}))\rho(\mathbf{r})d^3\mathbf{r} + \sum_{I<J}\frac{Z_I Z_J}{R_{IJ}}, \quad (1)$$

where $H_{\mu\nu}$ and $\rho_{\mu\nu}$ are the Hamiltonian density matrices in the PAO representation; Z_I is the valence ion pseudo-atom charge of the Ith atom; $V^H(\mathrm{r})$ is the Hartree potential distribution

$$\rho(\mathbf{r}) = \sum_{\mu\nu}\rho_{\mu\nu}\phi_\mu(\mathbf{r})\phi^*_\nu(\mathbf{r}) \quad (2)$$

is the electron density distribution obtained by transforming the density operator from the PAO representation into the Cartesian representation; $\phi_\mu(\mathbf{r})$ is the μth PAO; $\epsilon^{xc}(\mathbf{r})\rho(\mathbf{r})$ is the exchange-correlation energy distribution; and $V^{xc}(\mathbf{r})$ is the exchange-correlation potential distribution.

Using the two-center scheme of energy decomposition,[40] the total energy can be written as

$$E = \sum_{IJ} B_{IJ} + \sum_{I\neq J} C_{IJ}, \quad (3)$$

with electronic contribution

$$B_{IJ} = \sum_{\mu\in I,\,\nu\in J}\rho_{\mu\nu}\left(H_{\mu\nu} - \frac{1}{2}M^H_{\mu\nu} + M^{xc}_{\mu\nu}\right), \quad (4)$$

and ionic contribution

$$C_{IJ} = \frac{1}{2}\frac{Z_I Z_J}{R_{IJ}}. \quad (5)$$

While the ionic contribution can be calculated using the Ewald summation based on periodic boundary conditions,[41] the electronic contribution can be obtained from the DFT calculation results.[38] Here, the Hartree part

$$M^H_{\mu\nu} = \left\langle \phi_\mu | V^H | \phi_\nu \right\rangle \quad (6)$$

and the exchange-correlation part

$$M^{xc}_{\mu\nu} = \left\langle \phi_\mu | (\epsilon^{xc} - V^{xc}) | \phi_\nu \right\rangle \quad (7)$$

of the electronic contribution are obtained by modifying the output module in SIESTA.[38] This energy decomposition scheme serves as a powerful tool to quantitatively analyze the energy cost of bond formation

$$e_{IJ} = B_{IJ} + B_{JI} + C_{IJ} + C_{JI}, \quad (8)$$

where e_{IJ} refers to the bonding energy between atoms I and J.[40]

It worth noting that the bonding energy, e_{IJ}, is not the bond dissociation energy.[42] Instead, e_{IJ} is a component of the system's total energy, based on the energy decomposition scheme.[40] It can be used to quantitatively analyze the relative bonding strength between different atomistic building blocks of the system. When activated by thermal energy, melting typically starts at the location where the bonds are weakest.

C. Optical property analysis

The optical properties (dielectric constants) are analyzed using the method implemented in the SIESTA package. The calculation uses the simplest approach based on evaluating the dipolar transition matrix elements between different eigen-functions of the SCF converged Hamiltonian.[38]

D. *Ab initio* molecular dynamics

The AIMD simulations, based on DFT potential energy surfaces, are also performed using the SIESTA package.[38] The GeTe supercell contains 128 Ge and Te atoms, total.

The Gamma point is used to sample the Brillouin zone, due to the large size of the supercells.

During the AIMD simulations, the system's desired temperature, T, and pressure, P, are regulated by velocity rescaling and scaling of the supercell size and shape. Here, we set $P = 0$ Pa to enable isothermal, isobaric simulations—also referred to as NPT simulations. The time step is chosen to be 5 fs. For each temperature, T, the NPT AIMD simulation lasts for at least 30 ps. The temperature-dependent total energy is obtained by averaging the fluctuating total energy over the last 5 ps of simulation time.

Using melt-quench AIMD simulations, the a-PCM model is generated as follows: the c-PCM supercell is first heated at 1200 K for 15 ps—much higher than the c-PCM melting temperature (998 K for GeTe[14])—in order to destroy the crystalline lattice structure. Then, the liquid PCM is quenched to room temperature (300 K) over 15 ps. Finally, the PCM atomic coordinates are relaxed using the CG method until residual forces on all atoms are smaller than the convergence criterion of 40 meV/Å.

E. Finite element method

Based on the method introduced in our previous PCM study,[9] device performance can be obtained by solving the heat transfer equation

$$c_v \frac{\partial T}{\partial t} = \kappa \nabla^2 T + \rho_e J^2, \tag{9}$$

and Poisson equation, using TD-FEM, as implemented in the FreeFEM package.[43] Here, $T = T(\mathbf{r},t)$ is the temperature at position $\mathbf{r}$ and time t. J is the current density. The material constants c_v, κ, and ρ_e are the specific heat capacity, thermal conductivity, and electrical resistivity, respectively.

III. RESULTS

Results from applying the methodology introduced in Sec. II are presented in this section. First, by using *ab initio* DFT and the energy decomposition scheme (from Secs. II A and II B), the electronic structure and bonding energy are analyzed in Secs. III A and III B. Then, using DFT-based NPT AIMD simulations (from Sec. II D), the lattice structure, total system energy, melting temperature, specific heat capacity, and latent heat of fusion are quantitatively analyzed in Secs. III C–III G. Finally, using the DFT and AIMD results, the device performance metrics "reset" energy and dielectric constant are analyzed in Secs. III H and III I.

A. Electronic structure

The bandgap of c-GeTe is computed to be 0.24 eV,[19] which is in reasonable agreement with the measured value of 0.20 eV.[44] The two-dimensional electron density of pristine (undoped) c-GeTe and Bi-doped c-GeTe is shown in Fig. 1, where the well-known Peierls distortion can be observed clearly in pristine c-GeTe.[45] The electron density is much higher in regions with strong Ge-Te bonds than in regions with weak bonds. In the Bi-doped c-GeTe, the electron density distribution is significantly modified by the Bi dopant atom. The order of the strong/weak Ge-Te bonds is destroyed in the vicinity of the dopant atom. In this paper, we have explored the impact of doping on bonding energy of a limited number of materials. The general applicability of the bonding energy hierarchy analysis to phase change materials deserves further attention.

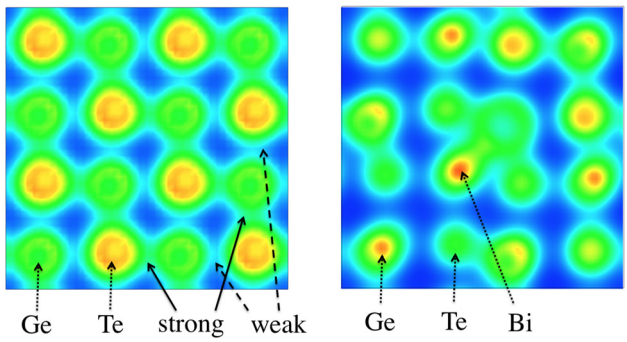


FIG. 1. Two-dimensional slice of electron density in pristine rhombohedral crystalline GeTe (left) and Bi-doped GeTe (right), obtained from pseudopotential DFT calculations. Due to the Peierls distortion, some Ge-Te bonds are strong, and some Ge-Te bonds are weak in the pristine crystalline GeTe.

B. Hierarchical bonding energy

To quantitatively analyze the dopant atom's impact on the bonding energy, the energy decomposition scheme (Sec. II B) is applied. We note that while the energy decomposition scheme is widely used in molecular analysis,[40,42,46,47] its use in the analysis of bulk materials is less common. We first apply the energy decomposition scheme to crystalline silicon, germanium, and tin. The Si-Si, Ge-Ge, and Sn-Sn bonding energies are calculated to be E_{Si}=1.53 eV, E_{Ge}=1.38 eV, and E_{Sn}=1.12 eV, respectively. It is known that the melting temperatures of the crystalline silicon, germanium, and tin are T_{Si}=1414 °C, T_{Ge}=938 °C, and T_{Sn}=232 °C, respectively.[48] The simulated relation $E_{\mathrm{Si}} > E_{\mathrm{Ge}} > E_{\mathrm{Sn}}$ agrees with the measured relation $T_{\mathrm{Si}} > T_{\mathrm{Ge}} > T_{\mathrm{Sn}}$, indicating that stronger bonds are related to higher melting temperatures.

For pristine c-GeTe, the bonding energies of the strong and weak bonds are computed to be $E_{\mathrm{GeTe(S)}} = 1.76$ eV and $E_{\mathrm{GeTe(W)}} = 0.70$ eV, respectively. When dopants are introduced, this difference in bonding energy associated with the two distinct (strong and weak) bonds is destroyed. As shown in Figs. 1 and 2, though Bi-doping strengthens some bonds, it weakens other bonds. There are many bonds that are weaker than $E_{\mathrm{GeTe(W)}}$ as shown in Fig. 2(b). During thermally activated lattice vibrations, these bonds are vulnerable defects in the crystalline PCM lattice, which could help reduce the melting temperature.

To explore the generality of the energy decomposition method, we analyze another prototypical PCM, antimony telluride (Sb_2Te_3). We find that the bonding energy of the weakest Sb-Te bond in the Sb_2Te_3 lattice is $E_{\mathrm{SbTe(W)}} = 0.42$ eV, lower than the weakest bond in GeTe of $E_{\mathrm{GeTe(W)}} = 0.70$ eV. The relation $E_{\mathrm{SbTe(W)}} < E_{\mathrm{GeTe(W)}}$ is in line with the measured fact that the melting temperature of Sb_2Te_3 (893 K) is lower than that of the GeTe (998 K).[14] Though we have investigated only a limited number of

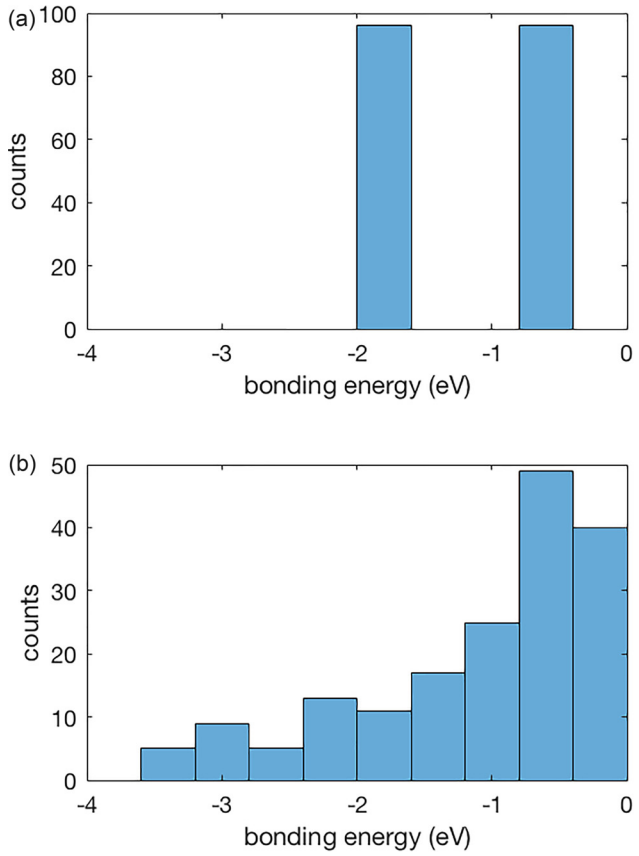


FIG. 2. Statistical distribution of the Ge-Te bonding energies of the pristine rhombohedral crystalline GeTe (a) and the Bi-doped GeTe, computed using the energy decomposition method. In (b), the bonds are taken from a cube (edge length 1.2 nm) in the vicinity of the Bi dopant atom. Here, the negative sign of the energy stems from that zero is selected as the reference energy level.

dopant concentrations to demonstrate the applicability of the proposed methodology, further comparison to AIMD at a larger variety of doping concentrations is required.

C. Lattice structure

To directly investigate the melting process, the NPT AIMD method (Sec. II D) is applied. Local snapshots of the GeTe lattice structures during melting are shown in Fig. 3. Similarly, the melting process of the Bi-doped GeTe can be simulated.

D. System total energy

The total system energy as a function of time is shown for three temperatures in Fig. 4(a). When the AIMD thermostat temperature is lower than 1000 K, the system remains crystalline due to strong bonds (Fig. 1) and the fluctuation in energy is small. When the AIMD thermostat temperature is further increased [e.g., 1040 K in Fig. 4(a)], bonding energies can no longer withstand the increased thermal vibrations and the crystalline order is destroyed. At this temperature, the system is melted into a higher-energy liquid phase. The higher the AIMD thermostat temperature, the faster is the melting process, as shown in Fig. 4(a).

Doping-facilitated melting can be clearly observed in Fig. 4(b). Under the same AIMD thermostat temperature of $T = 1000$ K, pristine c-GeTe keeps its crystalline lattice order for more than 30 ps [Fig. 2(a)]. However, due to presence of doping-induced vulnerable lattice spots [Fig. 2(b)], Bi-doped c-GeTe starts to melt within the first 10 ps and full melting is accomplished within 30 ps.

E. Melting temperature

The doping-induced decrease in melting temperature can be directly observed in Fig. 5. Without doping, the melting temperature of c-GeTe is simulated to be about $T_m \approx 1030$ K, which is slightly higher than the measured value 998 K due to superheating effects, where it is well known that the simulated melting temperature of a crystalline material is typically higher than the measured melting temperature. It is worth noting that this superheating effect is captured in our AIMD simulations. When doped with one Bi atom in the 128-atom c-GeTe supercell, the melting temperature becomes $T_m \approx 990$ K. The doping-induced decrease in the melting temperature is $\Delta T_m \approx 40$ K.

F. Latent heat of fusion

During PCM heating and melting, the "reset" operation energy consists of two parts—"sensible" energy to increase the kinetic energy/temperature, and "latent" energy to break the bonds and achieve phase transition. As shown in Fig. 5, during melting, there is an abrupt change of the total energy (H_{GeTe} and $H_{\mathrm{Bi\text{-}GeTe}}$), corresponding to the latent heat of fusion. The result shows that the Bi-doping decreases the latent heat of fusion by around 21.2%, i.e., $(H_{\mathrm{Bi\text{-}GeTe}} - H_{\mathrm{GeTe}})/H_{\mathrm{GeTe}} \approx -21.2\%$. This trend is in line with the bonding energy analysis results in Secs. III A and III B—during phase transition, it takes less energy to break the weakened bonds after doping.

Technologically, this trend is desirable to reduce the "reset" energy consumption. However, since latent heat of fusion consumes only a very small portion of the total "reset" energy, this trend exerts limited impact on the "reset" operation energy cost.[9]

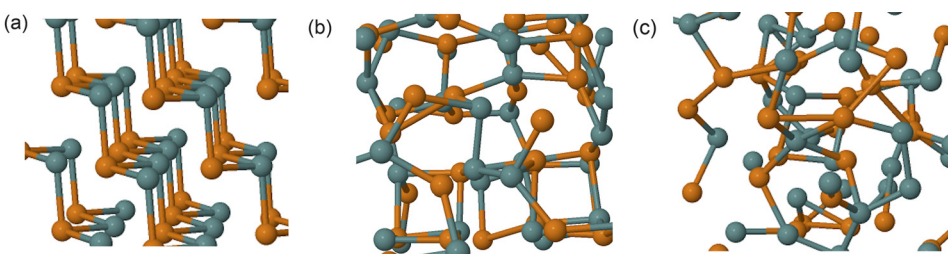


FIG. 3. Local snapshots of the atomistic coordinates of rhombohedral crystalline GeTe with Peierls distortion (a), the atomic coordinates of GeTe during the melting process (b), and the atomic coordinates of the liquid GeTe after the melting is accomplished (c).

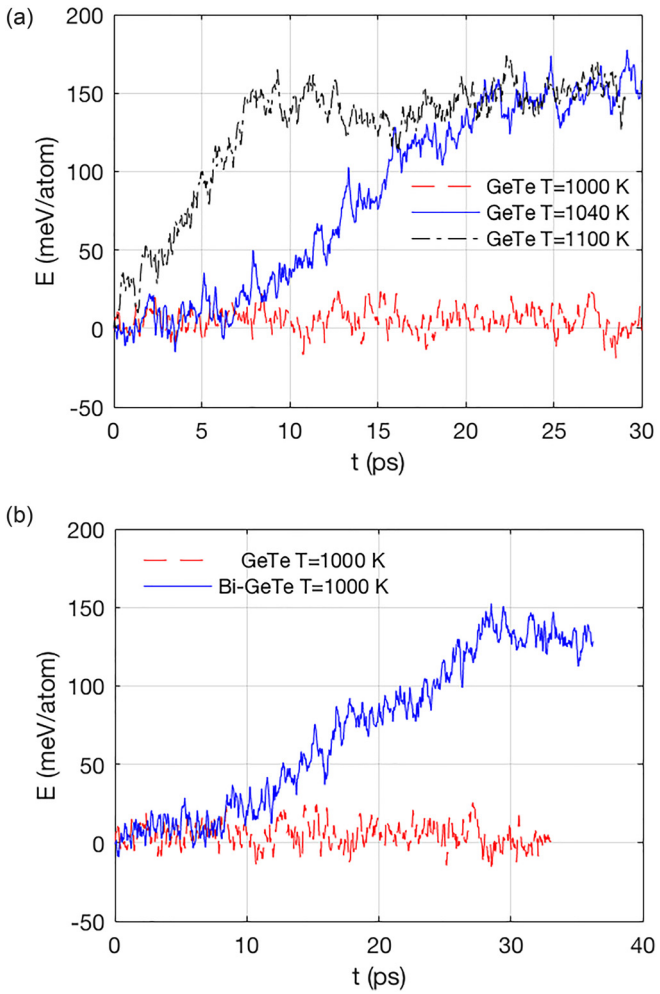


FIG. 4. The time-dependent evolution of the total system energy, E, of GeTe during the melting process, obtained by using the DFT-based NPT AIMD simulations. (a) The temperature-dependent total energy of undoped GeTe as a function of time. (b) The impact of Bi-dopant on the melting process when the AIMD simulation temperature, T, is set at 1000 K.

G. Specific heat capacity

The portion of "reset" energy used to increase the kinetic energy leads to an increase in temperature. Using the slope of the energy versus temperature relationship before melting, shown in Fig. 5, it can be estimated that the specific heat capacity increases by around 3.8% due to doping. Specific heat capacity is directly related to the degrees of freedom (DOF) available in the material to store energy.[49] In doped PCMs, the destruction of lattice order and bonding energy hierarchy (Figs. 1 and 2) increases the available DOF and results in higher specific heat capacity. However, the small doping-induced increase in specific heat capacity minimally impacts the total energy required for "reset," since specific heat capacity plays only a minor role.[9] The details to compute the specific heat capacity can be found in our prior work.[49]

H. RESET operation energy

In the TD-FEM solution of undoped GeTe, we use the following GeTe material parameters: c_v=1.6 J/m^{3}K;[50,51] κ=4.4 W/mK;[14] $\rho_e = 4.78 \times 10^{-6}$ Ωm; and latent heat of fusion oef 1.45 GJ/m^3. The other settings are kept the same as our prior study.[9] The simulated "reset" energy cost is $C_{\mathrm{GeTe}} \approx 1.66$ pJ.

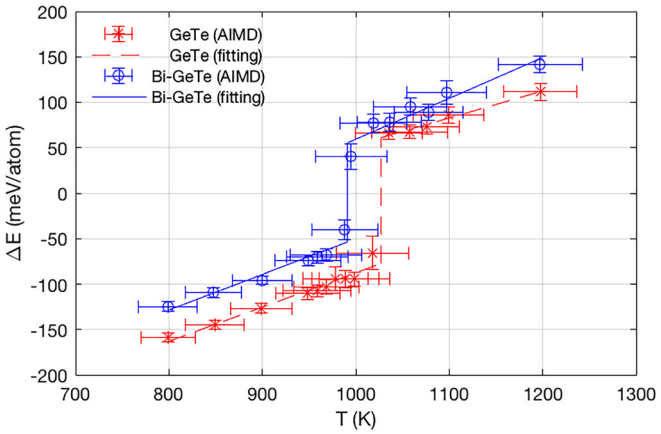


FIG. 5. The impact of Bi-doping on the melting of GeTe, where the horizontal/vertical bar represents the range of temperature/energy fluctuation for the NPT AIMD simulation; ΔT_m is the doping-induced decrease in melting temperature; and $H_{\mathrm{GeTe}}/H_{\mathrm{Bi\text{-}GeTe}}$ represents the change in total energy due to the latent heat of fusion of undoped/Bi-doped GeTe.

The reduction in melting temperature of $\Delta T_m \approx 40$ K (Sec. III E), the 21.2% decrease in latent heat of fusion (Sec. III F), and the 3.8% increase in specific heat capacity (Sec. III G) in Bi-doped GeTe are incorporated in the simulation. The TD-FEM results show that these doping-induced changes decrease the "reset" energy to $C_{\mathrm{Bi\text{-}GeTe}} \approx 1.56$ pJ. This 6% decrease in "reset" energy serves only as a lower bound to the doping-induced reduction of "reset" energy. In practice, the "reset" energy can be further reduced by doping.

First, due to limited computational resources, the AIMD simulation time is restricted to 30 ps. In real devices, the "reset" operation pulse is much longer. At a temperature value where AIMD shows no melting, a real sample of doped PCM may still achieve melting due to more thermal vibration attempts in breaking weakened bonds. Additionally, the doping could significantly suppress the thermal conductivity via electron and phonon scattering, effectively decreasing the "reset" energy.[9,11] In our simulations, the thermal conductivity of doped PCM was assumed to be unchanged compared to pristine PCM, because such effects have yet to be quantitatively characterized in experiment. Finally, the electrical resistivity could be significantly enhanced by doping, increasing the local joule heating, and facilitating efficient melting, but this effect is not considered here.

I. Optical properties

The optical property of interest is the complex dielectric constant $\epsilon = \epsilon_1 + i\epsilon_2$. The calculated results are shown in Fig. 6 and agree with the experimentally measured spectrum shown in Fig. 1 of Ref. 52. These simulations show that Bi-doping does not significantly influence the contrast of optical properties between the a-GeTe and the resonantly bonded c-GeTe,[53] which is essential for optical PCM devices to store data in a non-volatile manner.

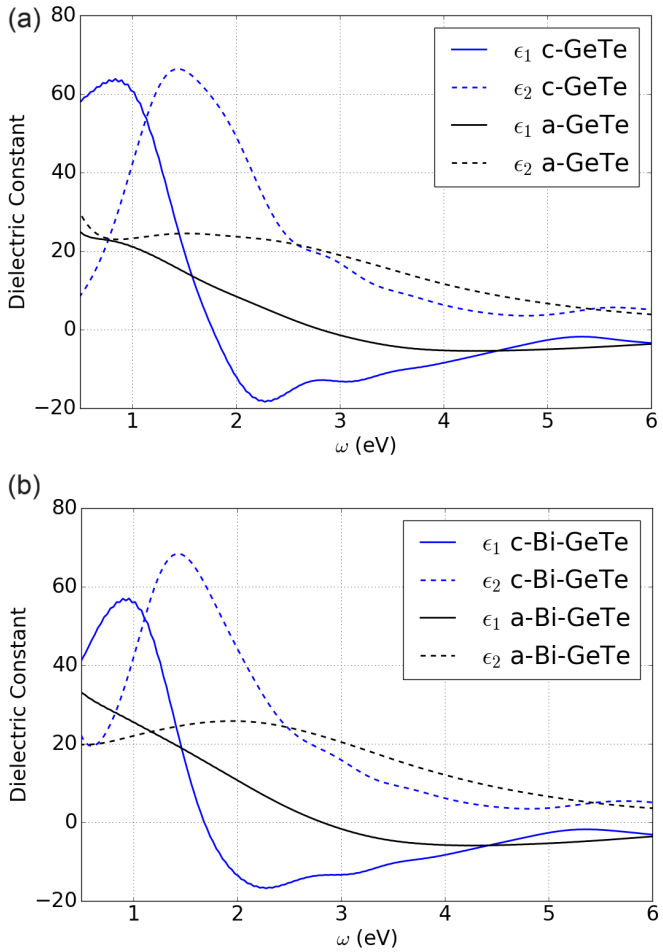


FIG. 6. Dielectric constant $\epsilon = \epsilon_1 + i\epsilon_2$ of the crystalline ($c-$) and amorphous ($a-$) undoped/Bi-doped (GeTe/Bi-GeTe) computed using DFT electronic structure results.

IV. COMPUTATIONAL COST

While both DFT-based bonding energy analyses (Secs. III A and III B) and AIMD methods (Secs. III C–III E) are both capable of capturing the relationship between doping and melting, the former is $t_0/dt \approx 10^3$–10^4 times less computationally demanding than the later, where t_0 is the total AIMD simulation time and dt is the AIMD timestep. Here, the estimation is done by using the typical melting simulation settings $t_0 \approx 10^1 - 10^2$ ps and $dt \approx 5$ fs.[20,33–35,49,54–57]

As mentioned in Sec. I, this drastic reduction in computational cost is critical for next-generation PCM design based on high-throughput simulations.[36] Proper application of this technique could allow for efficient analyses of dopant/material combinations in the search for reduced PCM "reset" energies. However, it deserves noting that the bonding energy analysis cannot offer insights into the dynamic lattice properties (e.g., atomistic vibrations) which AIMD can offer.

V. DISCUSSION

At present, in both electrical and optical PCM devices, switching from c-PCM to a-PCM is mainly based on melt-quench amorphization via Joule heating and fundamentally requires high "reset" energy consumption. Truly low "reset" energy consumption requires non-melting amorphization where current/laser pulses are carefully engineered to target only weaker bonds in the material.[45,47] The hierarchical bonding energy method discussed here may serve as a powerful tool for designing such devices.

The bonding energy analysis method presented here not only delivers promising reductions in computational cost, also the statistical distribution of the bonding energies in Fig. 2(b) may be used to quantitatively predict the melting temperature after doping. This type of application remains an open question and deserves future attention.

VI. CONCLUSION

In this paper, the impacts of doping on the bonding energy hierarchy, melting temperature, latent heat of fusion, specific heat capacity, optical properties, and "reset" energy consumption are analyzed. The atomic scale mechanisms underlying these impacts are investigated.

It is shown that Bi-doping can significantly reduce both the melting temperature and latent heat of fusion of c-GeTe, effectively reducing the "reset" energy consumption. Though Bi-doping slightly increases the specific heat capacity of c-GeTe, specific heat capacity carries minimal influence on the melting process and overall device performance. It is shown that after Bi-doping, the contrast of optical properties between c-GeTe and a-GeTe is still maintained, which is important for reliable non-volatile data storage.

The energy decomposition scheme is used to compute the bonding energies of prototypical phase change materials. It is found that, for the same type of material, the melting temperature, $T_{(m)}$, is related to the bonding energy of the weakest bond, $E_{(W)}$. For example, the simulated relation $E_{SbTe(W)} < E_{GeTe(W)}$ is in line with the measured relation that $T_{SbTe(m)} < T_{GeTe(m)}$; the simulated relation $E_{Bi\text{-}GeTe(W)} < E_{GeTe(W)}$ agrees with the measured relation $T_{Bi\text{-}GeTe(m)} < T_{GeTe(m)}$; and the simulated relation $E_{Sn(W)} < E_{Ge(W)} < E_{Si(W)}$ agrees with the measured relation $T_{Sn(m)} < T_{Ge(m)} < T_{Si(m)}$. Here, the subscripts "GeTe," "Bi-GeTe," "SbTe," "Sn," "Ge," and "Si" represent pristine crystalline germanium telluride (c-GeTe), Bi-doped c-GeTe, antimony telluride (Sb_2Te_3), tin, germanium, and silicon, respectively. It worth stressing that the above-mentioned relation between the bonding energy and the melting temperature is based on simulation results of a limited number of materials. To implement phase change memory devices, there are many material choices other than Ge-Sb-Te, e.g., Ga-Sb-Te[58] and Sc-Sb-Te.[1] The general applicability of the proposed methodology to these and other phase change materials deserves attention. Furthermore, doping induces vacancies, which may play an important role in the amorphization processes. The development of a quantitative methodology to study the impact of vacancies will be useful.

Finally, compared to the widely used *ab initio* molecular dynamics method of analyzing the melting process, bonding energy analysis is as much as 3–4 orders of magnitude more computationally efficient. This is a necessary improvement for the next-generation high-throughput simulation-based design process required to reduce PCM "reset" energy consumption.

ACKNOWLEDGMENTS

This research was supported by the Fundamental Research Funds for the Central Universities from Hunan University, Changsha, People's Republic of China, the United States National Science Foundation (NSF) under Grant Award Nos. 1005793, 1006182, and 1231927, and the funding from HRL, Inc., Malibu, CA, USA. The calculations were performed at the National Supercomputing Center in Changsha, People's Republic of China. This work used the Extreme Science and Engineering Discovery Environment (XSEDE), which is supported by the National Science Foundation (Grant No. OCI-1053575). This work was facilitated through the use of advanced computational, storage, and networking infrastructure provided by the Hyak supercomputer system, supported in part by the University of Washington's eScience Institute. We would like to thank Dr. Xianzhong Duan, Dr. Min He, Dr. Kenli Li, and Dr. Can Leng for their help. We thank Professor Sunil Patil for his comments on a draft of the manuscript.

[1]F. Rao, K. Ding, Y. Zhou, Y. Zheng, M. Xia, S. Lv, Z. Song, S. Feng, I. Ronneberger, R. Mazzarello, W. Zhang, and E. Ma, "Reducing the stochasticity of crystal nucleation to enable subnanosecond memory writing," Science **358**(6369), 1423–1427 (2017).

[2]D. Loke, T. H. Lee, W. J. Wang, L. P. Shi, R. Zhao, Y. C. Yeo, T. C. Chong, and S. R. Elliott, "Breaking the speed limits of phase-change memory," Science **336**(6088), 1566–1569 (2012).

[3]S. Kim, B.-J. Bae, Y. Zhang, R. Jeyasingh, Y. Kim, I.-G. Baek, S. Park, S.-W. Nam, and H.-S. Wong, "One-dimensional thickness scaling study of phase change material($Ge_2Sb_2Te_5$) using a pseudo 3-terminal device," IEEE Trans. Electron Devices **58**(5), 1483–1489 (2011).

[4]R. E. Simpson, M. Krbal, P. Fons, A. V. Kolobov, J. Tominaga, T. Uruga, and H. Tanida, "Toward the ultimate limit of phase change in $Ge_2Sb_2Te_5$," Nano Lett. **10**(2), 414–419 (2010).

[5]M. A. Caldwell, S. Raoux, R. Y. Wang, H.-S. Philip Wong, and D. J. Milliron, "Synthesis and size-dependent crystallization of colloidal germanium telluride nanoparticles," J. Mater. Chem. **20**(7), 1285–1291 (2010).

[6]T. Siegrist, P. Jost, H. Volker, M. Woda, P. Merkelbach, C. Schlockermann, and M. Wuttig, "Disorder-induced localization in crystalline phase-change materials," Nat. Mater. **10**(3), 202–208 (2011).

[7]H.-S. P. Wong, S. Raoux, S. Kim, J. Liang, J. P. Reifenberg, B. Rajendran, M. Asheghi, and K. E. Goodson, "Phase change memory," Proc. IEEE **98**(12), 2201–2227 (2010).

[8]S. Raoux, in *Phase Change Materials: Science and Applications*, edited by S. Raoux and M. Wuttig (Springer-Verlag GMBH, 2008).

[9]J. Liu, B. Yu, and M. P. Anantram, "Scaling analysis of nanowire phase-change memory," IEEE Electron Device Lett. **32**(10), 1340–1342 (2011).

[10]A. Pirovano, A. Lacaita, A. Benvenuti, F. Pellizzer, S. Hudgens, and R. Bez, "Scaling analysis of phase-change memory technology," in *Technical Digest of IEEE International Electron Devices Meeting* (2003), pp. 29.6.1–29.6.4.

[11]S. Kim and H.-S. Wong, "Analysis of temperature in phase change memory scaling," IEEE Electron Device Lett. **28**(8), 697–699 (2007).

[12]G. Atwood, "Engineering: Phase-change materials for electronic memories," Science **321**(5886), 210–211 (2008).

[13]See https://en.wikipedia.org/wiki/3D_XPoint for information about 3D XPoint non-volatile memory.

[14]B. Yu, X. Sun, S. Ju, D. Janes, and M. Meyyappan, "Chalcogenide-nanowire-based phase change memory," IEEE Trans. Nanotechnol. **7**(4), 496–502 (2008).

[15]J. Reifenberg, D. Kencke, and K. Goodson, "The impact of thermal boundary resistance in phase-change memory devices," IEEE Electron Device Lett. **29**(10), 1112–1114 (2008).

[16]J. Reifenberg, K.-W. Chang, M. Panzer, S. Kim, J. Rowlette, M. Asheghi, H.-S. Wong, and K. Goodson, "Thermal boundary resistance measurements for phase-change memory devices," IEEE Electron Device Lett. **31**(1), 56–58 (2010).

[17]F. Xiong, A. Liao, D. Estrada, and E. Pop, "Low-power switching of phase-change materials with carbon nanotube electrodes," Science **332**, 568–570 (2011).

[18]E. Simpson, P. Fons, V. Kolobov, T. Fukaya, M. Krbal, T. Yagi, and J. Tominaga, "Interfacial phase-change memory," Nat. Nano **6**, 501–505 (2011).

[19]J. Liu, "Multiscale simulation of phase change memory," Ph.D. dissertation (University of Washington, 2013).

[20]J. Liu, "A multi-scale analysis of the impact of pressure on melting of crystalline phase change material germanium telluride," Appl. Phys. Lett. **105**(17), 173509 (2014).

[21]M. Krbal, A. V. Kolobov, J. Haines, A. Pradel, M. Ribes, P. Fons, J. Tominaga, C. Levelut, R. Le Parc, and M. Hanfland, "Temperature independence of pressure-induced amorphization of the phase-change memory alloy $Ge_2Sb_2Te_5$," Appl. Phys. Lett. **93**(3), 031918 (2008).

[22]S. Kozyukhin, A. Sherchenkov, A. Babich, P. Lazarenko, H. P. Nguyen, and O. Prikhodko, "Peculiarities of bi doping of GeSbTe thin films for PCM devices," Can. J. Phys. **92**(7/8), 684–689 (2014).

[23]B. Qiao, J. Feng, Y. Lai, Y. Ling, Y. Lin, T. Tang, B. Cai, and B. Chen, "Effects of Si doping on the structural and electrical properties of $Ge_2Sb_2Te_5$ films for phase change random access memory," Appl. Surf. Sci. **252**(24), 8404–8409 (2006).

[24]A. Babich, A. Sherchenkov, S. Kozyukhin, P. Lazarenko, O. Boytsova, and A. Shuliatyev, "Effect of doping on the crystallization kinetics of phase change memory materials on the basis of GeSbTe system," J. Therm. Anal. Calorim. **127**(1), 283–290 (2017).

[25]K. B. Borisenko, Y. Chen, S. A. Song, and D. J. H. Cockayne, "Nanoscale phase separation and building blocks of $Ge_2Sb_2Te_5N$ and $Ge_2Sb_2Te_5N_2$ thin films," Chem. Mater. **21**(21), 5244–5251 (2009).

[26]M. S. Kim, S. H. Cho, S. K. Hong, J. S. Roh, and D. J. Choi, "Crystallization characteristics of nitrogen-doped Sb_2Te_3 films for PRAM application," Ceram. Int. **34**(4), 1043–1046 (2008).

[27]S. Privitera, E. Rimini, and R. Zonca, "Amorphous-to-crystal transition of nitrogen- and oxygen-doped $Ge_2Sb_2Te_5$ films studied by in situ resistance measurements," Appl. Phys. Lett. **85**(15), 3044–3046 (2004).

[28]S. Raoux, D. Cabrera, A. Devasia, S. Kurinec, H. Cheng, Y. Zhu, C. Breslin, J. Jordan-Sweet, C. T. Rettner, G. W. Burr, and M. Salinga. "Influence of dopants on the crystallization temperature, crystal structure, resistance, and threshold field for $Ge_2Sb_2Te_5$ and GeTe phase change materials," in *EPCOS* (2011).

[29]K. Wang, C. Steimer, D. Wamwangi, S. Ziegler, and M. Wuttig, "Effect of indium doping on $Ge_2Sb_2Te_5$ thin films for phase-change optical storage," Appl. Phys. A **80**(8), 1611–1616 (2005).

[30]J. Zhang, R. Huang, L. Shi, L. Wang, F. Wei, T. Kong, and G. Cheng, "Bi doping modulating structure and phase-change properties of GeTe nanowires," Appl. Phys. Lett. **102**(6), 063104 (2013).

[31]J. Zhou, Z. Sun, L. Xu, and R. Ahuja, "Effect of dopants on the structure and properties of $Ge_2Sb_2Te_5$ studied by ab initio calculations," Solid State Commun. **148**(3–4), 113–116 (2008).

[32]X. Zhou, L. Wu, Z. Song, F. Rao, M. Zhu, C. Peng, D. Yao, S. Song, B. Liu, and S. Feng, "Carbon-doped $Ge_2Sb_2Te_5$ phase change material: A candidate for high-density phase change memory application," Appl. Phys. Lett. **101**(14), 142104 (2012).

[33]J. Akola and R. O. Jones, "Comment on 'formation of large voids in the amorphous phase-change memory $Ge_2Sb_2Te_5$ alloy'," Phys. Rev. Lett. **104**(1), 019603 (2010).

[34]J. Akola and R. O. Jones, "Binary alloys of Ge and Te: Order, voids, and the eutectic composition," Phys. Rev. Lett. **100**(20), 205502 (2008).

[35]T. Matsunaga, J. Akola, S. Kohara, T. Honma, K. Kobayashi, E. Ikenaga, R. O. Jones, N. Yamada, M. Takata, and R. Kojima, "From local structure to nanosecond recrystallization dynamics in AgInSbTe phase-change materials," Nat. Mater. **10**(2), 129–134 (2011).

[36]N. Mounet, M. Gibertini, P. Schwaller, D. Campi, A. Merkys, A. Marrazzo, T. Sohier, I. E. Castelli, A. Cepellotti, G. Pizzi, and N. Marzari, "Two-dimensional materials from high-throughput computational exfoliation of experimentally known compounds," Nat. Nanotechnol. **13**(3), 246–252 (2018).

[37]M. Wuttig and N. Yamada, "Phase-change materials for rewriteable data storage," Nat. Mater. **6**(11), 824–832 (2007).

[38]J. M. Soler, E. Artacho, J. D. Gale, A. Garca, J. Junquera, P. Ordejon, and S.-P. Daniel, "The SIESTA method for ab initio order- N materials simulation," J. Phys.: Condens. Matter **14**(11), 2745–2779 (2002).

[39]J. P. Perdew, K. Burke, and M. Ernzerhof, "Generalized gradient approximation made simple," Phys. Rev. Lett. **77**(18), 3865–3868 (1996).

[40]I. Mayer, "An exact chemical decomposition scheme for the molecular energy," Chem. Phys. Lett. **382**, 265–269 (2003).
[41]R. M. Martin, *Electronic Structure Basic Theory and Practical Method* (Cambridge University Press, Cambridge, UK, 2004).
[42]R. T. Sanderson, "Interrelation of bond dissociation energies and contributing bond energies," J. Am. Chem. Soc. **97**(6), 1367–1372 (1975).
[43]F. Hecht, "New development in freefem++," J. Numer. Math. **20**(3–4), 251–266 (2012).
[44]L. L. Chang, P. J. Stiles, and L. Esaki, "Electron barriers in Al-AL2O3-SnTe and Al-AL2O3-GeTe tunnel junctions," IBM J. Res. Develop. **10**(6), 484–486 (1966).
[45]A. V. Kolobov, M. Krbal, P. Fons, J. Tominaga, and T. Uruga, "Distortion-triggered loss of long-range order in solids with bonding energy hierarchy," Nat. Chem. **3**(4), 311–316 (2011).
[46]T.-Y. Lai, C.-Y. Yang, H.-J. Lin, C.-Y. Yang, and W.-P. Hu, "Benchmark of density functional theory methods on the prediction of bond energies and bond distances of noble-gas containing molecules," J. Chem. Phys. **134**(24), 244110 (2011).
[47]R. J. Levis, "Selective bond dissociation and rearrangement with optimally tailored, strong-field laser pulses," Science **292**(5517), 709–713 (2001).
[48]See http://www.ioffe.ru/ for information about the melting temperatures of the crystalline silicon, germanium, and tin.
[49]J. Liu, X. Xu, L. Brush, and M. P. Anantram, "A multi-scale analysis of the crystallization of amorphous germanium telluride using ab initio simulations and classical crystallization theory," J. Appl. Phys. **115**(2), 023513 (2014).
[50]R. Shaltaf, X. Gonze, M. Cardona, R. K. Kremer, and G. Siegle, "Lattice dynamics and specific heat of alpha-GeTe: Theoretical and experimental study," Phys. Rev. B **79**(7), 075204 (2009).
[51]V. M. Zhdanov, "Low temperature heat capacity, enthalpy, and entropy of germanium telluride," Russ. J. Phys. Chem. **45**, 1357 (1971).
[52]J.-W. Park, S. H. Eom, H. Lee, J. L. F. Da Silva, Y.-S. Kang, T.-Y. Lee, and Y. H. Khang, "Optical properties of pseudobinary GeTe, $Ge_2Sb_2Te_5$, $GeSb_2Te_4$, $GeSb_4Te_7$, and Sb_2Te_3 from ellipsometry and density functional theory," Phys. Rev. B **80**(11), 115209 (2009).
[53]K. Shportko, S. Kremers, M. Woda, D. Lencer, J. Robertson, and M. Wuttig, "Resonant bonding in crystalline phase-change materials," Nat. Mater. **7**(8), 653–658 (2008).
[54]J. Liu, X. Xu, and M. Anantram, "Role of inelastic electron-phonon scattering in electron transport through ultra-scaled amorphous phase change material nanostructures," J. Comput. Electron. **13**, 620–626 (2014).
[55]J. Liu, X. Xu, and M. Anantram, "Subthreshold electron transport properties of ultrascaled phase change memory," IEEE Electron Device Lett. **35**(5), 533–535 (2014).
[56]J. Liu and M. P. Anantram, "Low-bias electron transport properties of germanium telluride ultrathin films," J. Appl. Phys. **113**(6), 063711 (2013).
[57]J. Liu, "Microscopic origin of electron transport properties and ultrascalability of amorphous phase change material germanium telluride," IEEE Trans. Electron Devices **64**(5), 2207–2215 (2017).
[58]H.-Y. Cheng, K.-F. Kao, C.-M. Lee, and T.-S. Chin, "Crystallization kinetics of GaSbTe films for phase change memory," Thin Solid Films **516**(16), 5513–5517 (2008).